Elastic ^{16}O+^{20}Ne scattering from a folding model analysis

Yong-Xu Yang[1,*] and Qing-Run Li[2]

[1]*Department of Physics, Guangxi Normal University, Guilin 541004, People's Republic of China*

[2]*Institute of High Energy Physics, Chinese Academy of Sciences, Beijing 100039, People's Republic of China*

(Received 15 May 2011; published 6 July 2011)

A folding potential for elastic ^{16}O+^{20}Ne scattering is constructed based on the four-α-particle model for the ^{16}O nucleus and the α+^{16}O model for the ^{20}Ne nucleus. The elastic scattering angular distributions of the ^{16}O+^{20}Ne system in the energy range of $E_{\rm c.m.} = 24.5$–35.5 MeV are calculated by use of the α-folding potential obtained. The calculations show that the experimental data can be reasonably well described. The surface term in the imaginary potential has a significant effect on the calculations of the cross section at large angles for the energies considered.

DOI: 10.1103/PhysRevC.84.014602 PACS number(s): 25.70.Bc, 24.10.Ht, 21.60.Gx

I. INTRODUCTION

Elastic scattering between 4*N*-type nuclei has been extensively studied in the past decades. The measured cross sections for these systems often exhibit pronounced anomalous large-angle scattering (ALAS). The ALAS feature is prominent in ^{16}O+^{20}Ne scattering and has attracted considerable attention. In Ref. [1], the angular distributions for elastic and inelastic ^{16}O+^{20}Ne scattering at $E_{\rm c.m.} = 22.2$ MeV were measured and analyzed with an α cluster exchange process in the optical model, optical model plus distorted-wave Born approximation, and coupled-channel approaches. In Ref. [2], the angular distributions and excitation functions of elastic and inelastic ^{16}O+^{20}Ne scattering for $E_{\rm c.m.} = 9$–30 MeV were measured and studied in terms of α exchange, resonances, and statistical fluctuations. In particular, in Refs. [3–6], ^{16}O+^{20}Ne scattering data in the energy range of $E_{\rm c.m.} = 20$–40 MeV, which exhibit strong oscillation structures in the backward angle region, were extensively investigated by using the extended optical model and coupled-channel approaches. In these studies, the oscillation structures observed in angular distributions and excitation functions were well described using nucleus-nucleus potentials including both a parity-dependent real term and an angular-momentum-dependent absorptive part. In the earlier works of these studies [3,4], shallow potentials were used for the extended optical model and coupled-channel calculations and reasonable descriptions of the data were obtained. Later, in Refs. [5,6], with a deep real potential, the experimental angular distributions and excitation functions were also well described.

However, as far as we know, there have been numerous investigations of the scattering of 4*N*-type nuclei using diverse optical potentials which do not contain a parity-dependent real term and an angular-momentum-dependent absorptive part, and reasonably good descriptions to the experimental data have been obtained. But for the ^{16}O+^{20}Ne system, there are few investigations available using such parity- and angular-momentum-independent potentials. In Ref. [7], a parity- and angular-momentum-independent potential was developed by use of the iterative perturbative (IP) method for S(1)-to-V(r) inversion, and it led to the same angular distributions as those obtained using the phenomenological parity- and angular-momentum-dependent deep potential for the ^{16}O+^{20}Ne system in Ref. [6].

The folding model has been widely used to describe the optical potential for heavy-ion collisions. It has been shown that folding model potentials give a good account of the scattering between some 4*N*-type nuclei. For example, the ^{12}C+^{12}C, ^{16}O+^{12}C, ^{16}O+^{16}O, ^{12}C+^{24}Mg, ^{12}C+^{28}Si, and ^{16}O+^{28}Si elastic scattering data have been well described by folding potentials in diverse approaches [8–16]. However, for ^{16}O+^{20}Ne scattering, there is only one paper [17] involving a calculation using a folding potential; no other studies are available using a folding model to attempt to explain the ^{16}O+^{20}Ne scattering.

In this work, we present calculated results for elastic ^{16}O+^{20}Ne scattering obtained by using an α-folding model potential. From the perspective of nuclear cluster structure, ^{16}O and ^{20}Ne can be considered as 4α and α+^{16}O configurations. In our previous studies based on the four-α-particle model for the ^{16}O nucleus and the α+^{16}O model for the ^{20}Ne nucleus, we proposed α-folding potentials for the description of α+^{16}O, ^{16}O+^{16}O, and α+^{20}Ne elastic scattering [18–20]. The α-folding potentials obtained can well describe the experimental angular distributions of these systems at the incident energies considered. In the present work, we construct an α-folding potential for the analysis of elastic ^{16}O+^{20}Ne scattering to further examine the α-folding model potential and the α+^{16}O model of the ^{20}Ne nucleus. The strong ALAS feature observed in elastic ^{16}O+^{20}Ne scattering will be a stricter test of the model.

In the next section we present a brief outline of the α-folding potential for the description of elastic ^{16}O+^{20}Ne scattering. The calculated results, comparison with the experimental data, and discussion are given in the last section.

II. α-FOLDING POTENTIAL FOR THE ^{16}O+^{20}Ne SYSTEM

From the 4α model of the ^{16}O nucleus and the α+^{16}O model of ^{20}Ne nucleus, the real part of the optical potential

*yyxu@mailbox.gxnu.edu.cn

for the ^{16}O+^{20}Ne scattering can be represented by the folding potential

$$V(\mathbf{R}) = \int V_{\alpha^{20}\mathrm{Ne}}(\mathbf{R}-\mathbf{r})\rho_{\alpha}(\mathbf{r})\,d\mathbf{r}, \tag{1}$$

where $\rho_{\alpha}(\mathbf{r})$ is the α-particle density distribution in the ^{16}O nucleus. The interaction between an α particle and the target nucleus $V_{\alpha^{20}\mathrm{Ne}}(\mathbf{R})$ is also a folding potential:

$$V_{\alpha^{20}\mathrm{Ne}}(\mathbf{R}) = \int \left[V_{\alpha\alpha}\left(\mathbf{R}-\frac{4}{5}\mathbf{r}\right) + V_{\alpha^{16}\mathrm{O}}\left(\mathbf{R}+\frac{1}{5}\mathbf{r}\right)\right] \times |\chi_0(\mathbf{r})|^2 d\mathbf{r}, \tag{2}$$

with

$$V_{\alpha^{16}\mathrm{O}}(\mathbf{R}) = \int V_{\alpha\alpha}(\mathbf{R}-\mathbf{r})\rho_{\alpha}(\mathbf{r})\,d\mathbf{r}, \tag{3}$$

where $\chi_0(\mathbf{r})$ is the wave function for the relative motion of the α and ^{16}O clusters in the ground state of the ^{20}Ne nucleus, and $\mathbf{r}$ is the relative coordinate between the centers of mass of α and ^{16}O. The α-α interaction we used is that given by Buck *et al.* [21], that is,

$$V_{\alpha\alpha}(r) = -122.6225\exp(-0.22r^2)\ \mathrm{MeV}. \tag{4}$$

The form factor describing the α-particle distribution in the ^{16}O nucleus has been given in our previous work [19] as

$$\eta_{\alpha}(q) = \Theta(q)\left[1-\left(\frac{1}{6}+\frac{\sqrt{6}}{12}\right)(aq)^2+\frac{1}{48}(aq)^4\right]e^{-a^2q^2/4}, \tag{5}$$

where $a = 1.2$ fm is the harmonic-oscillator parameter, and $\Theta(q) = e^{a^2q^2/16}$ is the c.m. correction factor.

The above α-α potential and the α distribution form factor have been applied to construct the folding potentials for the α+^{16}O [18] and ^{16}O+^{16}O scattering [19], and the obtained potentials can satisfactorily describe the experimental angular distributions of the elastic α+^{16}O scattering at incident energies from 25 to 54 MeV and the elastic ^{16}O+^{16}O scattering at incident energies from 75 to 124 MeV.

For the α+^{16}O relative motion wave function $\chi_0(\mathbf{r})$ in expression (2), we have proposed an α+^{16}O model of the ^{20}Ne nucleus [20,22]. In this model the relative motion wave function for the ground state of the ^{20}Ne nucleus can be written as

$$\chi_0(\mathbf{r}) = R_0(r)Y_{00}(\theta,\phi), \tag{6}$$

where $R_0(r)$ is the radial wave function, and is given as

$$R_0(r) = \sin\frac{\beta}{2}O_{10}(r) + \cos\frac{\beta}{2}O_{20}(r). \tag{7}$$

Here $O_{10}(r)$ and $O_{20}(r)$ are the harmonic-oscillator radial functions with the quantum numbers $1s$ and $2s$, respectively, that is,

$$O_{10}(r) = 2(a^6\pi)^{-1/4}e^{-r^2/2a^2} \tag{8}$$

and

$$O_{20}(r) = \sqrt{\frac{8}{3}}(a^6\pi)^{-1/4}\left[\frac{3}{2}-\left(\frac{r}{a}\right)^2\right]e^{-r^2/2a^2}. \tag{9}$$

By fitting the experimental charge form factor of ^{20}Ne, we obtain the parameters $a = 1.96$ fm and $\beta = 282.4^{\circ}$.

Using the relative motion wave function $\chi_0(\mathbf{r})$ and the α-^{16}O potential $V_{\alpha^{16}\mathrm{O}}(\mathbf{R})$ provided in [18], the folding potential $V_{\alpha^{20}\mathrm{Ne}}(\mathbf{R})$ of expression (2) can be easily obtained and expressed as an analytical function. This folding potential has been applied to describe the elastic α+^{20}Ne scattering and can yield a reasonable description of the experimental angular distributions for incident energies of 31.1, 54.1, and 104.0 MeV [20].

Because of the analytical and simple forms of $V_{\alpha\alpha}(r)$, $\eta_{\alpha}(q)$, $\chi_0(\mathbf{r})$, $V_{\alpha^{16}\mathrm{O}}(\mathbf{R})$, and $V_{\alpha^{20}\mathrm{Ne}}(\mathbf{R})$, the folding model potential of expression (1) can be conveniently obtained and expressed as an analytical function. Then, as in the usual folding model calculations, the total optical potential used to describe the elastic ^{16}O+^{20}Ne scattering has the form

$$U(R) = NV(R) + W(R) + V_C(R), \tag{10}$$

where N is the renormalization factor and $W(R)$ is the imaginary part of the interaction. The Coulomb potential $V_C(R)$ is taken to correspond to a uniformly charged sphere of radius $R_C = 1.3(A_1^{1/3}+A_2^{1/3})$.

For the imaginary part of the potential, two choices were used, a pure volume term of standard Woods-Saxon (WS) type and the volume term together with an additional surface term of a Woods-Saxon derivative (WSD) shape:

$$W(R) = \frac{-iW_0}{1+\exp\left(\frac{R-R_W}{a_W}\right)} \tag{11}$$

and

$$W(R) = \frac{-iW_0}{1+\exp\left(\frac{R-R_W}{a_W}\right)} + \frac{-i4W_D\exp\left(\frac{R-R_D}{a_D}\right)}{\left[1+\exp\left(\frac{R-R_D}{a_D}\right)\right]^2}, \tag{12}$$

with $R_{W,D} = r_{W,D}(A_1^{1/3}+A_2^{1/3})$.

III. RESULTS AND DISCUSSION

The available experimental data [4] of elastic ^{16}O+^{20}Ne scattering in the energy range of $E_{\mathrm{c.m.}} = 24.5$–35.5 MeV have been analyzed using the α-folding model potential constructed in Sec. II. To investigate the predictive ability of the α-folding potential, the imaginary potential should be chosen as simple as possible to show the predominant effect of the real part. Thus we use a simple standard Woods-Saxon-type imaginary potential for our first investigation. And to reduce the number of free parameters, the radius parameter $r_W = 1.30$ fm and the diffuseness $a_W = 0.70$ fm were chosen and fixed in the whole investigated energy range; only two parameters N and W_0 were adjusted to obtain a fit to the experimental data. The calculated angular distributions are shown in Fig. 1 in comparison with the experimental data. The corresponding values of N, W_0, and the volume integrals of the real and the imaginary potentials are listed in Table I.

From Fig. 1, one can see that the α-folding potential with a simple standard Woods-Saxon imaginary part can overall describe the main features of the elastic ^{16}O+^{20}Ne scattering angular distributions. The behavior of the backward

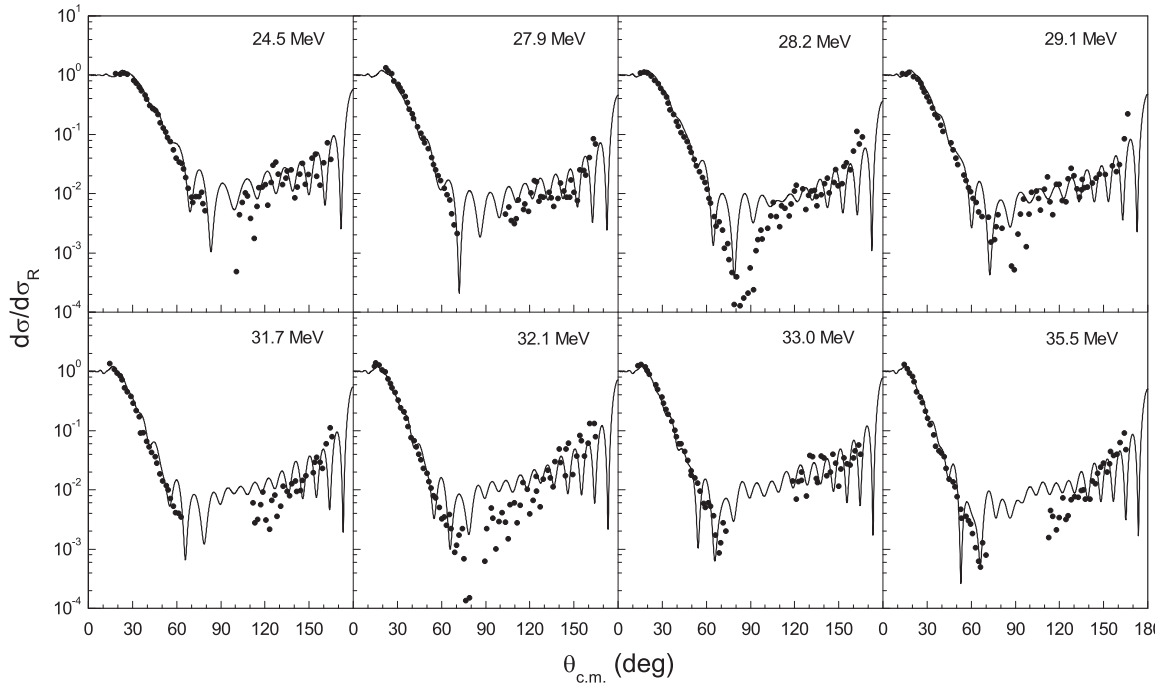

FIG. 1. The angular distributions of elastic $^{16}O+^{20}Ne$ scattering at energies of $E_{c.m.} = 24.5, 27.9, 28.2, 29.1, 31.7, 32.1\ 33.0$, and 35.5 MeV. The curves show the calculated results by use of the α-folding potential with a WS imaginary part. The experimental data are taken from Ref. [4].

rise is reproduced to a certain extent, but the predictions for the backward angles are not satisfying. Especially for the energies of $E_{c.m.} = 28.2$, 29.1, 31.7, 32.1, and 35.5 MeV, the calculations overestimate the data at angles $\theta_{c.m.} \approx 80^\circ$–$120^\circ$ and underestimate the data at larger angles. However, the calculations show that the α-folding model potential, which has a deep real part and is parity independent, has general predictive ability to explain the angular distributions of elastic $^{16}O+^{20}Ne$ scattering. We expect that the quality of the fit would be improved by using a more flexible imaginary potential.

Analyses for the $^{16}O+^{12}C$ and $^{16}O+^{16}O$ systems [11,12,23] have shown that for the data at higher energies an acceptable description was possible using just a volume term for the imaginary part, whereas the fits at lower energies (lower than $E_{c.m.} = 40$ MeV) required inclusion of a surface imaginary term. And in Ref. [24], for analysis of the $^{16}O+^{28}Si$ system using a deep modified optical potential with an imaginary potential consisting of the sum of a Woods-Saxon volume and a surface potential, it was observed that the surface term had a significant effect at all the energies considered. As in the present investigation for elastic $^{16}O+^{20}Ne$ scattering, the energy range is $E_{c.m.} = 24.5$–35.5 MeV, where the surface imaginary term may play an important role. Thus, we use an imaginary potential consisting of a WS volume term plus a WSD surface term for further analysis. In Ref. [23], it was found that the volume diffuseness of the imaginary potential tends to be very small when the surface imaginary term is included in the potential. The volume imaginary diffuseness can be fixed at some small value, such as 0.1 fm. In Ref. [24], the radius parameter found for the volume imaginary term is $R_W = 0.060\,84 E_{c.m.} - 0.544$ fm, which is much smaller than that generally used for lower energies.

TABLE I. Values of the renormalization factor, the central depth of the imaginary potential, and the volume integrals of the real and imaginary potentials for calculations using a WS imaginary part with $r_W = 1.30$ fm and $a_W = 0.70$ fm.

$E_{c.m.}$ (MeV)	N	W_0 (MeV)	J_R/A_1A_2 (MeV fm^3)	J_I/A_1A_2 (MeV fm^3)
24.5	1.13	5.5	467.8	25.1
27.9	1.10	6.3	455.4	28.7
28.2	1.05	6.4	434.7	29.2
29.1	1.09	6.4	451.3	29.2
31.7	1.14	6.8	472.0	31.0
32.1	1.14	6.6	472.0	30.1
33.0	1.14	6.7	472.0	30.5
35.5	1.14	7.4	472.0	33.7

In our calculations, referring to the above works [11,12,23,24] and after several attempts, the parameters $r_W = 0.24$ fm, $a_W = 0.10$ fm, $r_D = 1.08$ fm, and $a_D = 0.60$ fm were chosen and fixed in the whole considered energy range; only N, W_0, and W_D were allowed to vary to obtain a fit to the experimental data. The calculated results are shown in Fig. 2 in comparison with experimental data. The obtained values of the renormalization factor N, the central depths W_0 and W_D of the imaginary potential, and the volume integrals of the real and the imaginary potentials are listed in Table II. One can see that much better fits to the data are obtained by using an imaginary potential with a WS volume term plus a WSD surface term than by using only a WS volume term. The backward rise and

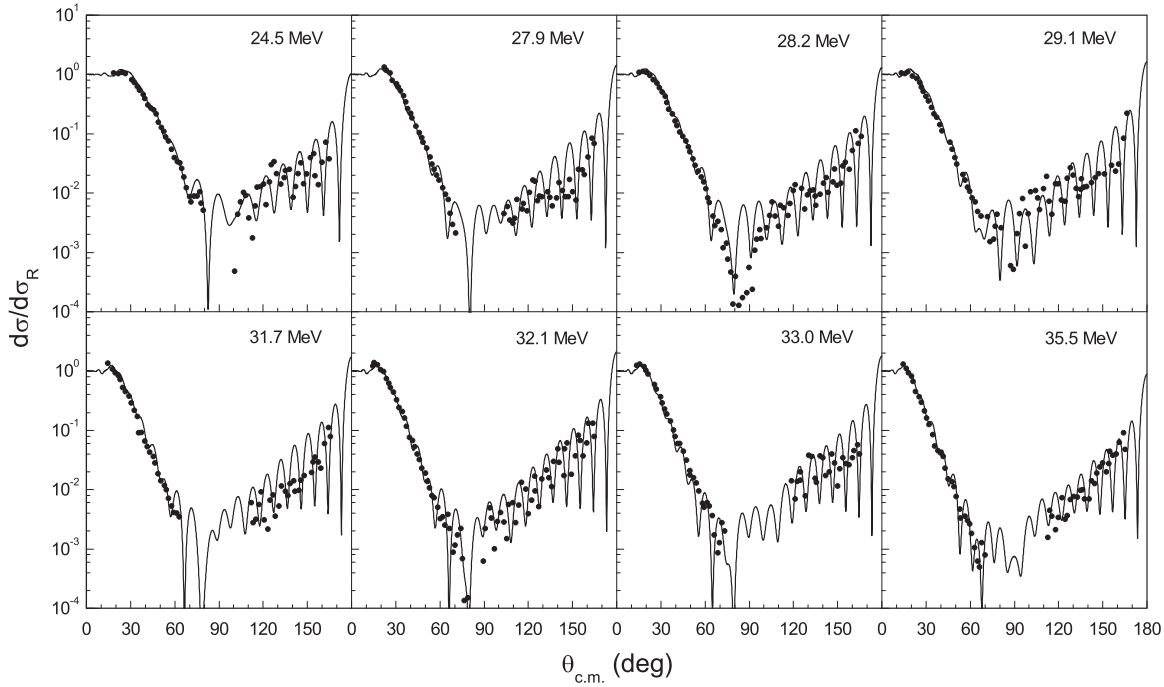

FIG. 2. As Fig. 1, but for the WS + WSD imaginary potential.

the oscillatory structure are well described by the calculations. However, the calculations are somewhat out of phase with the measurements and overestimate the data at some angles for some incident energies.

From the obtained parameters listed in Table II, the required renormalization factors are $N \approx 1.15 \pm 0.01$. The volume integrals of the real potential are very weakly dependent on energy in this energy range, while the imaginary volume integrals increase with incident energy. The obtained real volume integrals $J_R/A_1A_2 \approx 475 \pm 5$ MeV fm^3 are "anomalously" strong comparing to those of "normal" potentials for neighboring 4*N*-type nuclei systems. For the ^{12}C+^{12}C, ^{16}O+^{12}C, and ^{16}O+^{16}O systems, Brandan and Satchler [10] extracted the values of the volume integrals as a function of projectile energy per nucleon for various potentials that fit the data (see Fig. 6.7 of Ref. [10]). It is shown that the real volume integrals are less than 400 MeV fm^3.

TABLE II. Values of the renormaliztion factor, the central depths of the WS and the WSD terms, and the volume integrals of the real and imaginary potentials for calculations using the WS + WSD imaginary part with $r_W = 0.24$ fm, $a_W = 0.10$ fm, $r_D = 1.08$ fm, and $a_D = 0.60$ fm.

$E_{\text{c.m.}}$ (MeV)	N	W_0 (MeV)	W_D (MeV)	J_R/A_1A_2 (MeV fm^3)	J_I/A_1A_2 (MeV fm^3)
24.5	1.14	42.0	6.0	472.0	19.9
27.9	1.15	49.0	7.0	476.1	23.2
28.2	1.16	52.0	7.2	480.2	23.9
29.1	1.15	53.0	7.2	476.1	24.0
31.7	1.14	54.0	8.0	472.0	26.5
32.1	1.14	55.0	8.0	472.0	26.5
33.0	1.15	56.0	8.6	476.1	28.4
35.5	1.15	56.0	10.6	476.1	34.7

It should be pointed out that the anomaly of the stronger real volume integral was revealed in α elastic scattering on ^{20}Ne [20,25,26]. It has been shown that a normal real potential with volume integral J_R/A_1A_2 around 350 MeV fm^3 can well reproduce the experimental cross sections for α scattering on lower-mass targets [25], but fails to describe the data for the ^{20}Ne target. Michel and Reidemeister [26] found that, for the 54.1 MeV elastic α+^{20}Ne scattering, a phenomenological potential with real volume integral about 500 MeV fm^3 can well describe the backward angle enhancement of the data but is unable to obtain a satisfactory phasing with the data for the whole angular range. However, the data can be quantitatively described by use of a real potential with J_R/A_1A_2 about 350 MeV fm^3 plus a small parity-dependent real part. In our previous analysis of the elastic α+^{20}Ne scattering based on a framework similar to the present α-folding model, the required volume integrals for the real potential to get a fit to the data are about 450–490 MeV fm^3 [20].

It seems that the potential for the description of elastic ^{16}O+^{20}Ne scattering, like that for α+^{20}Ne scattering, has different properties from the normal potentials. In Refs. [3–6], an extended potential with a parity-dependent real term and an angular-momentum-dependent absorptive part can reasonably describe the elastic ^{16}O+^{20}Ne scattering data. Here, the data have been well described by an α-folding model potential with a much stronger real volume integral than that of a normal potential. However, the quality of the fits for the angular distributions obtained via the α-folding model potential shown here in Fig. 2 is better than that obtained by the parity- and angular-momentum-dependent extended optical potentials shown in Refs. [3–5]. In

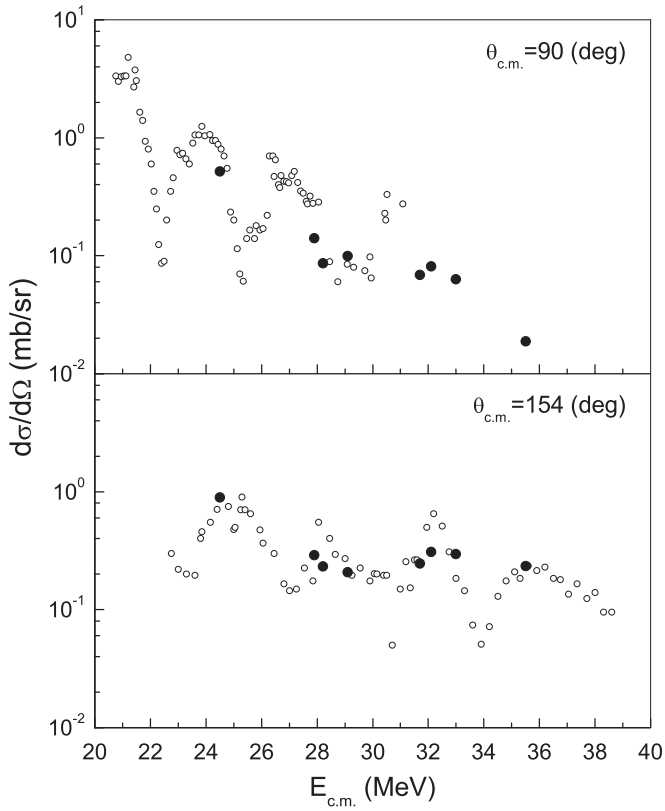

FIG. 3. Excitation function for elastic ^{16}O+^{20}Ne scattering at $\theta_{\text{c.m.}} = 90^\circ$ and 154°. The solid circles are calculations averaged over an angular range of $\pm 2^\circ$ for the considered energies obtained by the α-folding potential with a WS + WSD imaginary part. The data (open circles) are taken from Refs. [27,28].

Ref. [7], the parity- and angular-momentum-independent potential obtained by using the IP inversion method gave the same angular distributions as the phenomenological parity- and angular-momentum-dependent "deep" potential in Ref. [6]. The real part of this potential in Ref. [7] is deeper and exhibits some oscillations, and the absorptive part is surface transparent, having a small and energy-dependent radius.

In Ref. [17], calculations for the 32.1 MeV elastic ^{16}O+^{20}Ne scattering show that the M3Y double-folding model potential cannot describe the data at backward angles, whereas the data can be well described by including an α-transfer amplitude in the elastic channel. In this case, the α-exchange effect makes a significant contribution to the large-angle cross sections. In our present analysis, we have not explicitly taken account of the exchange effect between the incident and target α particles, which is beyond the folding model framework. We consider that, since the α-α potential given by Buck *et al.* takes into account the indistinguishability of two α particles, the exchange effect may be partly included in the α-folding model through the α-α potential. Therefore, the backward rise can be well reproduced by the obtained α-folding potential. However, from the analyses in Ref. [17], it may be expected that the inclusion of the accurate α-exchange process will yield a better description of the phase and magnitude of the backward oscillations.

For the ^{16}O+^{20}Ne system, there are experimental elastic excitation functions at $\theta_{\text{c.m.}} = 90^\circ$ and 154° [27,28]. In Fig. 3, we show the values of the cross section averaged over an angular range of $\pm 2^\circ$ calculated by the α-folding model, together with the experimental data. One can see that the calculated cross sections are in general agreement with the experimental data for the considered energies. However, to obtain a full description of the excitation functions, an expression for the energy dependence of the optical potential should be established. In particular, from the experience of the previous relevant studies, the energy dependence of the imaginary potential should be reasonably well known. In Refs. [3–5,27], an angular-momentum- and energy-dependent imaginary potential is introduced for the ^{16}O+^{20}Ne system, and a reasonable description of the excitation functions is obtained. In this work, we do not attempt to obtain a practicable expression for the energy dependence of the optical potential. The intention of the present work, as mentioned above, is to examine the α-folding model potential and the α+^{16}O model of the ^{20}Ne nucleus via elastic ^{16}O+^{20}Ne scattering. This simple α-folding model with only two or three free parameters can obtain the results shown in Figs. 1–3. Thus the aim of the present study has been well achieved.

In summary, based on the four-α-particle model for the ^{16}O nucleus and the α+^{16}O model for the ^{20}Ne nucleus, we have constructed a folding model potential to describe elastic ^{16}O+^{20}Ne scattering. The available experimental elastic ^{16}O+^{20}Ne scattering data in the energy range of $E_{\text{c.m.}} = 24.5$–35.5 MeV have been analyzed by use of this α-folding potential. The calculated results show that, with a simple standard WS imaginary part, the α-folding potential can only give a qualitative description of the data, whereas, with an imaginary potential consisting of a WS volume term plus a WSD surface term, the experimental data can been reasonably well described. The ALAS feature and the oscillatory structure are well reproduced although detailed fits to the values and the phase of the data at backward angles are not very satisfactory. The required renormalization factor is $N \approx 1.15 \pm 0.01$ to get a good fit to the data, which leads to an anomalously stronger real volume integral of $J_R/A_1A_2 \approx 475 \pm 5$ MeV fm^3. The anomaly of the ^{16}O+^{20}Ne scattering should be further systematically studied.

ACKNOWLEDGMENT

The research is supported by the National Natural Science Foundation of China under Grant No. 10865002.

[1] R. Stock, U. Jahnke, D. L. Hendrie, J. Mahoney, C. F. Maguire, W. F. W. Schneider, D. K. Scott, and G. Wolschin, Phys. Rev. C **14**, 1824 (1976).

[2] M. Gai, G. M. Berkowitz, P. Braun-Munzinger, C. M. Jachcinski, C. E. Ordoñez, T. R. Renner, and C. D. Uhlhorn, Phys. Rev. C **30**, 925 (1984).

[3] Y. Kondō, B. A. Robson, and R. Smith, Nucl. Phys. A **410**, 289 (1983).
[4] Y. Kondō, B. A. Robson, and R. Smith, Nucl. Phys. A **437**, 117 (1985).
[5] C. Gao, Y. Kondō, and B. A. Robson, Nucl. Phys. A **529**, 234 (1991).
[6] Chengqun Gao and Guozhu He, Phys. Lett. B **282**, 16 (1992).
[7] S. Ait-Tahar, R. S. Mackintosh, and S. G. Cooper, Nucl. Phys. A **561**, 285 (1993).
[8] R. G. Stokstad, R. M. Wieland, G. R. Satchler, C. B. Fulmer, D. C. Hensley, S. Raman, L. D. Rickertsen, A. H. Snell, and P. H. Stelson, Phys. Rev. C **20**, 655 (1979).
[9] Li Qing-Run and Yang Yong-Xu, Phys. Rev. C **47**, 2393 (1993).
[10] M. E. Brandan and G. R. Satchler, Phys. Rep. **285**, 143 (1997), and references therein.
[11] M. P. Nicoli *et al.*, Phys. Rev. C **60**, 064608 (1999).
[12] M. P. Nicoli, F. Haas, R. M. Freeman, S. Szilner, Z. Basrak, A. Morsad, G. R. Satchler, and M. E. Brandan, Phys. Rev. C **61**, 034609 (2000).
[13] Dao T. Khoa, W. von Oertzen, H. G. Bohlen, and F. Nuoffer, Nucl. Phys. A **672**, 387 (2000).
[14] M. Karakoc and I. Boztosun, Phys. Rev. C **73**, 047601 (2006).
[15] T. Furumoto, Y. Sakuragi, and Y. Yamamoto, Phys. Rev. C **80**, 044614 (2009).
[16] G. Kocak, M. Karakoc, I. Boztosun, and A. B. Balantekin, Phys. Rev. C **81**, 024615 (2010).
[17] A. A. Farra, Turkish Journal of Physics **22**, 895 (1998).
[18] Q. R. Li and Y. X. Yang, Nucl. Phys. A **561**, 181 (1993).
[19] Y. X. Yang and Q. R. Li, Phys. Rev. C **72**, 054603 (2005).
[20] Y. X. Yang, H. L. Tan, and Q. R. Li, Phys. Rev. C **82**, 024607 (2010).
[21] B. Buck, H. Friedrich, and C. Wheathly, Nucl. Phys. A **275**, 246 (1977).
[22] P. T. Ong, Y. X. Yang, and Q. R. Li, Eur. Phys. J. A **41**, 229 (2009).
[23] S. Szilner, M. P. Nicoli, Z. Basrak, R. M. Freeman, F. Haas, A. Morsad, M. E. Brandan, and G. R. Satchler, Phys. Rev. C **64**, 064614 (2001).
[24] I. Boztosun, Phys. Rev. C **66**, 024610 (2002).
[25] H. Abele *et al.*, Z. Phys. A **326**, 373 (1987).
[26] F. Michel and G. Reidemeister, Z. Phys. A **333**, 331 (1989).
[27] D. F. Hebbard, J. Nurzynski, T. R. Ophel, P. V. Drumm, Y. Kondō, B. A. Robson, and R. Smith, Nucl. Phys. A **481**, 161 (1988).
[28] J. Schimizu *et al.*, Phys. Lett. B **112**, 323 (1982).